Strong Mixed-Integer Formulations for Transmission Expansion Planning with FACTS Devices

Kevin Wu, Mathieu Tanneau, Pascal Van Hentenryck
Georgia Institute of Technology, Atlanta, GA, United States
kwu381@gatech.edu, {mathieu.tanneau, pascal.vanhentenryck}@isye.gatech.edu

***Abstract*—Transmission Network Expansion Planning (TNEP) problems find the most economical way of expanding a given grid given long-term growth in generation capacity and demand patterns. The recent development of Flexible AC Transmission System (FACTS) devices, which can dynamically re-route power flows by adjusting individual branches' impedance, call for their integration into TNEP problems. However, the resulting TNEP+FACTS formulations are significantly harder to solve than traditional TNEP instances, due to the nonlinearity of FACTS behavior. This paper proposes a new mixed-integer formulation for TNEP+FACTS, which directly represents the change in power flow induced by individual FACTS devices. The proposed formulation uses an extended formulation and facet-defining constraints, which are stronger than big-M constraints typically used in the literature. The paper conducts numerical experiments on a synthetic model of the Texas system with high renewable penetration. The results demonstrate the computational superiority of the proposed approach, which achieves a 4x speedup over state-of-the-art formulations, and highlight the potential of FACTS devices to mitigate congestion.**

***Index Terms*—transmission expansion planning, FACTS**

NOMENCLATURE

a) Sets:

$\mathcal{N}$	Set of buses; $\mathcal{N} = \{1, ..., N\}$
$\mathcal{E}$	Set of branches; $\mathcal{E} = \{1, ..., E\}$
$\mathcal{S}$	Set of scenarios; $\mathcal{S} = \{1, ..., S\}$

b) Parameters:

$\mathbf{p}^{\text{d}}_{i,s}$	Load at node $i \in \mathcal{N}$ in scenario $s \in \mathcal{S}$
$\underline{\mathbf{p}}^{\text{g}}_{i,s}, \bar{\mathbf{p}}^{\text{g}}_{i,s}$	min/max output of generator $i \in \mathcal{N}$ in scenario $s \in \mathcal{S}$
c^{cap}_{ij}	Line capacity upgrade cost of edge $ij \in \mathcal{E}$
c^{TCSC}_{ij}	TCSC installation cost on edge $ij \in \mathcal{E}$
c_i	Production cost function of generator i
λ	Power balance violation penalty cost
Δ^c	Capacity upgrade increment (MW) of branches
m	Number of capacity upgrade increments available
X_{ij}	Reactance of branch $ij \in \mathcal{E}$
$\bar{\mathbf{p}}^{\text{f}}_{ij}$	Thermal limit of branch $ij \in \mathcal{E}$
$\underline{\theta}_{ij}, \bar{\theta}_{ij}$	min/max angle difference on branch $ij \in \mathcal{E}$

c) Variables:

γ_{ij}	Capacity upgrade level of branch $ij \in \mathcal{E}$
ψ_{ij}	Whether a FACTS device is installed on branch $(i,j) \in \mathcal{E}$
$\theta_{i,s}$	Voltage angle of bus $i \in \mathcal{N}$ in scenario $s \in \mathcal{S}$
$\mathbf{p}^{\text{g}}_{i,s}$	Output of generator $i \in \mathcal{N}$ in scenario $s \in \mathcal{S}$
$\mathbf{p}^{\text{f}}_{ij,s}$	Power flow on branch $ij \in \mathcal{E}$ in scenario $s \in \mathcal{S}$
$\xi_{i,s}$	Power imbalance at bus $i \in \mathcal{N}$ in scenario $s \in \mathcal{S}$

I. INTRODUCTION

In order to accommodate a high penetration of renewable generation, especially wind and solar generation, existing power grids need substantial investments in transmission capacity [1]. This poses a challenge for transmission system operators (TSOs) who are responsible for the expansion of infrastructure that delivers power from generators to loads. This need naturally gives rise to Transmission Network Expansion Planning (TNEP) problems, which find the most economical way of expanding the grid given long-term growth in generation capacity and demand patterns [2]. TNEP problems are mixed-integer programming problems, which are notoriously hard to solve [2].

Recent years have also witnessed the development of so-called Flexible AC Transmission System (FACTS) devices, such as phase-shifting transformers (PSTs), Thrystor Controlled Series Compensators (TCSCs), and Static Synchronous Series Compensators (SSSCs), to name a few [3]. FACTS devices can dynamically re-route power flows across the grid by emulating a change in line impedances. It is therefore natural to include such technology in TNEP studies, which can lead to lower investment and operational costs, and improve the long-term reliability of the grid. However, TNEP problems with FACTS devices (TNEP+FACTS for short) have received little attention in the literature. *This paper addresses this gap by proposing new, improved mixed-integer linear programming (MILP) formulations for the TNEP+FACTS problem.*

A. Related Work

Because of its importance for long-term power systems operations, there is a rich body of works on TNEP problems and their solution, e.g., [4], [5], [6], [7]. TNEP problems may consider transmission expansion only, or combined generation and transmission expansion planning [4]. Power flow equations are typically linearized using the DC approximation, which

This research is partly funded by NSF award 2112533 and ARPA-E PERFORM award AR0001136.

yields MILP problems. Stochastic formulations of TNEP, e.g. two-stage stochastic programming formulations [5], [6], are also popular. Most state-of-the-art approaches use a form of Benders decomposition algorithm to solve TNEP efficiently. Readers are referred to [2] for a more exhaustive survey of TNEP problems. The paper focuses on TNEP+FACTS problems, which have received significantly less attention.

Several papers combine traditional TNEP methodologies with the deployment of FACTS devices [3], [8], [9], [10], [11], [12]. Mokhtari et al. [3] consider a distributionally robust formulation with linearized AC constraints, which is solved with a Benders' decomposition algorithm. A differential evolution-based metaheuristic algorithm is proposed in [8] for solving TNEP+FACTS with AC constraints. Also in the AC setting, Luburic et al. [9] consider a TNEP+FACTS formulation with TCSCs and energy storage, and report results on a 24-bus system. Esmaili et al. [10] consider a multi-stage, short circuit-constrained TNEP problem with TCSC and SFCL devices, which is executed on 39-bus and 118-bus systems. It should be noted that the studies mentioned above were conducted solely on small artificial test systems which may not capture the dynamics of real-life grids.

Ziaee et al. [11] consider the placement of TCSC devices within a TNEP framework in the DC setting. The TNEP+FACTS problem is modeled via a combination of big-M and third-order relaxation techniques, and experiments are reported on 6-bus and 118-bus systems. Franken et al. [12] propose an MILP formulation for TNEP+FACTS where the effect of FACTS devices is modeled as virtual phase shifts. The resulting disjunctive constraints are linearized using big-M constraints. Numerical results on a synthetic 120-bus system suggest that FACTS devices have the potential to reduce expansion costs, renewable curtailment, and load shedding. One limitation of the study in [12] is that the proposed TNEP+FACTS model considers only a single load/renewable scenario, which may fail to capture, e.g., seasonal variations in system conditions.

B. Contributions

The paper considers the integration of FACTS devices in the formulation and solution of TNEP problems, and makes the following contributions. First, it proposes to formulate for TNEP+FACTS using variables that directly represents the impact of FACTS devices on power flows, rather than using virtual angle shifts. Second, it introduces a strong MILP formulation for TNEP+FACTS using an extended formulation with facet-defining inequalities. Third, it conducts numerical experiments on the Texas system under a high penetration of renewable generation. *The results demonstrate that the proposed MILP formulation achieves significant speedups over current state-of-the-art formulations, with a 4x speedup and a 40x reduction in branch-and-bound nodes needed to prove optimality.* The experiments also provide some insights into the benefits of FACTS devices for long-term network expansion planning. In particular, *the results highlight the benefits of FACTS devices for expansion planning through flow control.*

Model 1 The TNEP formulation without FACTS devices

$$\begin{aligned} \min \quad & \sum_{ij\in\mathcal{E}} c^{\text{cap}}_{ij}\gamma_{ij} + \frac{1}{S}\sum_{i\in\mathcal{N},s\in\mathcal{S}} c_i(\mathbf{p}^{\text{g}}_{i,s}) + \lambda|\xi_{i,s}| \\ \text{s.t.} \quad & (1)-(2), \quad \forall i\in\mathcal{N}, s\in\mathcal{S} \\ & (3)-(5), \quad \forall ij\in\mathcal{E}, s\in\mathcal{S} \end{aligned}$$

Together, these results should encourage subsequent studies to include FACTS devices in their studies and adopt the strong formulation presented in the paper.

The rest of the paper is organized as follows. Section II describes the TNEP and TNEP+FACTS formulations considered in the paper, presents the proposed strong MILP formulation for TNEP+FACTS, and proves its theoretical properties. Section III presents a case study of TNEP+FACTS on a synthetic model of the Texas system, which demonstrates the computational advantages of the proposed formulation, and illustrates the benefits of FACTS devices on a real system. Section IV concludes the paper and highlights directions for future work.

II. Formulation

This section presents the TNEP formulations used in the paper. Section II-A presents the baseline TNEP formulation, which does not include FACTS devices. Section II-B presents an initial MILP formulation for TNEP+FACTS, based on [12], which includes FACTS devices like TCSCs. Section II-C presents the proposed strengthened MILP formulation for TNEP+FACTS, and proves theoretical guarantees for the quality of the formulation.

The presentation assumes, for ease of reading and without loss of generality, that exactly one generator is attached to each bus. Reference (slack) bus voltage constraints are also omitted for simplicity.

A. Baseline TNEP formulation

Model 1 presents the baseline TNEP formulation, whose variables, constraints and objective are described next.

1) Variables: An important feature of the paper's approach is the observation that, due to a combination of economic, political and social factors, new transmission lines are very uncommon. Therefore, *the paper only considers capacity upgrades for existing lines*, which are captured by investment variables γ_{ij} that denote, for each branch $ij\in\mathcal{E}$ the capacity upgrade level on that branch. Investment variables γ_{ij} are restricted to integer values, with up to m possible capacity upgrades for each line. Other variables in the problem include generation dispatches $\mathbf{p}^{\text{g}}$, nodal voltage angles θ, power flows $\mathbf{p}^{\text{f}}$, and nodal imbalance variables ξ.

2) Constraints: Power balance is enforced at each bus $i\in\mathcal{N}$ and scenario $s\in\mathcal{S}$ as follows:

$$\mathbf{p}^{\text{g}}_{i,s} + \sum_{ji\in\mathcal{E}} \mathbf{p}^{\text{f}}_{ji,s} - \sum_{ij\in\mathcal{E}} \mathbf{p}^{\text{f}}_{ij,s} = \mathbf{p}^{\text{d}}_{is} + \xi_{i,s}, \tag{1}$$

where slack variable ξ captures nodal power imbalances.

The generation minimum and maximum limits are enforced for each generator $i \in \mathcal{N}$ and scenario $s \in \mathcal{S}$ as

$$\underline{\mathbf{p}}^{\mathrm{g}}_{i,s} \leq \mathbf{p}^{\mathrm{g}}_{i,s} \leq \bar{\mathbf{p}}^{\mathrm{g}}_{i,s}. \tag{2}$$

Renewable (wind and solar) generators have a minimum output of 0, and their maximum output varies based on the scenario $s \in \mathcal{S}$. The minimum/maximum limits of non-renewable generators typically depend on the physical characteristics of the generator, and may vary between, e.g., summer and winter.

The power flow on branch $ij \in \mathcal{E}$ in scenario $s \in \mathcal{S}$ is determined by Ohm's law

$$\mathbf{p}^{\mathrm{f}}_{ij,s} = \frac{1}{X_{ij}}(\theta_{j,s} - \theta_{i,s}), \tag{3}$$

and must satisfy thermal limit constraints of the form

$$-\bar{\mathbf{p}}^{\mathrm{f}}_{ij} - \gamma_{ij}\Delta^{c}_{ij} \leq \mathbf{p}^{\mathrm{f}}_{ij,s} \leq \bar{\mathbf{p}}^{\mathrm{f}}_{ij} + \gamma_{ij}\Delta^{c}_{ij}. \tag{4}$$

The original thermal limit $\bar{\mathbf{p}}^{\mathrm{f}}_{ij}$ may be increased by upgrading the line, as captured by variable γ_{ij}. In addition, phase angle differences $\theta_{ij,s} = (\theta_{j,s} - \theta_{i,s})$ are constrained by

$$\underline{\theta}_{ij} \leq \theta_{ij,s} \leq \bar{\theta}_{ij}. \tag{5}$$

3) Objective: The TNEP objective minimizes up-front investment costs in capacity upgrades, plus operational costs that capture, for each scenario, generation costs and penalty costs for any unserved/overserved energy.

B. TNEP with FACTS devices

The paper also considers FACTS devices such as TCSCs, which can dynamically adjust the reactance of a line [3]. Binary $\psi_{ij} \in \{0, 1\}$ takes value 1 if a FACTS device is installed on branch ij, and 0 otherwise. If a FACTS device is installed on branch $ij \in \mathcal{E}$, i.e., if $\psi_{ij} = 1$, Ohm's law (3) in scenario $s \in \mathcal{S}$ becomes

$$\mathbf{p}^{\mathrm{f}}_{ij,s} = \frac{1}{X_{ij} + \delta X_{ij,s}}\theta_{ij,s}, \tag{6}$$

$$= (B_{ij} + \delta B_{ij,s})\theta_{ij,s}, \tag{7}$$

where variables $\delta X_{ij,s}$ and $\delta B_{ij,s}$ capture the change in reactance and susceptance induced by the FACTS device on branch ij in scenario s, where

$$\delta B_{ij,s} = \frac{-\delta X_{ij}}{X_{ij}(X_{ij} + \delta X_{ij})}. \tag{8}$$

Equation (7) can be written equivalently as

$$\mathbf{p}^{\mathrm{f}}_{ij,s} = B_{ij}\theta_{ij,s} + \delta\mathbf{p}^{\mathrm{f}}_{ij,s}, \tag{9}$$

where variable $\delta\mathbf{p}^{\mathrm{f}}_{ij,s} = \delta B_{ij,s}\theta_{ij,s}$ captures the change in power flow induced by the FACTS device.

Substituting out $\delta B_{ij,s} = (\delta\mathbf{p}^{\mathrm{f}}_{ij,s})\theta^{-1}_{ij,s}$ yields the disjunction

$$\delta\underline{B}_{ij}\theta_{ij,s} \leq \delta\mathbf{p}^{\mathrm{f}}_{ij,s} \leq \delta\bar{B}_{ij}\theta_{ij,s} \qquad \text{if } \theta_{ij,s} \geq 0, \tag{10a}$$

$$\delta\bar{B}_{ij}\theta_{ij,s} \leq \delta\mathbf{p}^{\mathrm{f}}_{ij,s} \leq \delta\underline{B}_{ij}\theta_{ij,s} \qquad \text{if } \theta_{ij,s} \leq 0, \tag{10b}$$

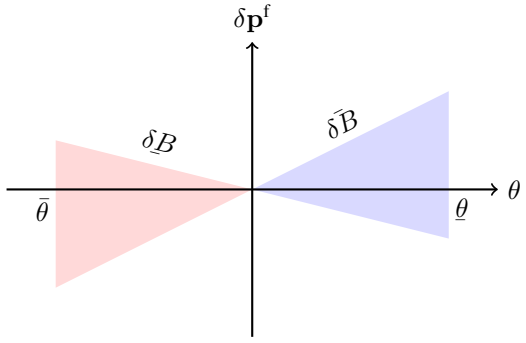

Fig. 1. Domain Space of $(\mathbf{p}^{\mathrm{f}}, \theta)$

Model 2 The baseline TNEP+FACTS formulation

$$\min \quad \sum_{ij\in\mathcal{E}} c^{\mathrm{cap}}_{ij}\gamma_{ij} + c^{\mathrm{TCSC}}_{ij}\psi_{ij} + \frac{1}{S}\sum_{i\in\mathcal{N},s\in\mathcal{S}} c_i(\mathbf{p}^{\mathrm{g}}_{i,s}) + \lambda|\xi_{i,s}|$$

$$\text{s.t.} \quad (1), (2) \quad \forall i \in \mathcal{N}, s \in \mathcal{S}$$
$$(4), (5), (9) \quad \forall ij \in \mathcal{E}, s \in \mathcal{S}$$
$$(11) - (14) \quad \forall ij \in \mathcal{E}, s \in \mathcal{S}$$
$$(15) \quad \forall ij \in \mathcal{E}, s \in \mathcal{S}$$

where $\delta\underline{B}_{ij}, \delta\bar{B}_{ij}$ are the minimum and maximum changes in susceptance induced by the FACTS device. The disjunction is illustrated in Figure 1. Franken et al. [12] represent the disjunction (10) via big-M constraints, and introduce binary variable $z_{ij,s}$ that takes value 1 if $\theta_{ij,s} \geq 0$ and 0 otherwise. This formulation reads

$$\delta\mathbf{p}^{\mathrm{f}}_{ij,s} \geq \delta\underline{B}_{ij}\theta_{ij,s} - M(1 - z_{ij,s}), \tag{11}$$

$$\delta\mathbf{p}^{\mathrm{f}}_{ij,s} \leq \delta\bar{B}_{ij}\theta_{ij,s} + M(1 - z_{ij,s}), \tag{12}$$

$$\delta\mathbf{p}^{\mathrm{f}}_{ij,s} \geq \delta\bar{B}_{ij}\theta_{ij,s} - Mz_{ij,s}, \tag{13}$$

$$\delta\mathbf{p}^{\mathrm{f}}_{ij,s} \leq \delta\underline{B}_{ij}\theta_{ij,s} + Mz_{ij,s}. \tag{14}$$

In addition, to ensure that power flows can only be modified when a FACT device is installed, [12] use the additional big-M constraint

$$-M\psi_{ij} \leq \delta\mathbf{p}^{\mathrm{f}}_{ij,s} \leq M\psi_{ij}. \tag{15}$$

The resulting TNEP+FACTS formulation is presented in Model 2. Note that the formulation stated in [12] does not use the $\delta\mathbf{p}^{\mathrm{f}}$ variables, but an equivalent angle representation.

The original presentation in [12] uses a single constant M for big-M constraints (11)–(15), whose value is not specified. A valid value for M is $\max_{ab\in\mathcal{E}}(\bar{\mathbf{p}}^{\mathrm{f}}_{ab} + m\Delta^{c})$. Tight big-M bounds are important in ensuring strong performance of MILP solvers. Therefore, this paper proposes to improve the approach of [12] by using a different big-M bound for each branch $M_{ij} = \bar{\mathbf{p}}^{\mathrm{f}}_{ij} + m\Delta^{c}$. This modified formulation uses the same variables and constraints as the formulation outlined in Model 2; only the big-M bounds are modified.

C. Strong MILP Formulation for TNEP+FACTS

While classical TNEP problems can be solved using Benders decomposition, this strategy is not applicable when considering FACTS devices because of the non-convexity of the disjunctions in (10). Instead, the TNEP+FACTS problem is solved directly using off-the-shelf MILP solvers. In that context, the formulation proposed by [12] has two main limitations. On the one hand, it relies on big-M constraints, which are notoriously detrimental to the performance of MILP solvers, because they typically lead to weak linear relaxations with highly fractional solutions. On the other hand, there is no direct link between binary variables ψ and z, with the latter introducing an un-necessary level of complexity when $\psi = 0$.

A key contribution of this paper is to address this limitation by proposing a strong MILP formulation for the TNEP+FACTS problem, which significantly improves solution time. The proposed formulation uses an extended formulation of the disjunctive constraints (10) using an additional binary variable, together with facet-defining inequalities. The strong formulation is presented for a fixed branch $ij \in \mathcal{E}$ and scenario $s \in \mathcal{S}$. For each of reading, the ij and s subscripts are dropped; note that θ thus denotes the angle difference $\theta_{ij,s} = \theta_{j,s} - \theta_{i,s}$.

First observe that, to capture the fact that $\delta\mathbf{p}^{\mathrm{f}} = 0$ if no FACTS device is installed, the 2-term disjunction in (10) can be extended to the 3-term disjunction

$$\delta\mathbf{p}^{\mathrm{f}} = 0 \qquad \text{if } \psi = 0, \tag{16a}$$
$$\delta\underline{B}\theta \le \delta\mathbf{p}^{\mathrm{f}} \le \delta\bar{B}\theta \qquad \text{if } \psi = 1 \text{ and } \theta \ge 0, \tag{16b}$$
$$\delta\bar{B}\theta \le \delta\mathbf{p}^{\mathrm{f}} \le \delta\underline{B}\theta \qquad \text{if } \psi = 1 \text{ and } \theta \le 0. \tag{16c}$$

This 3-term disjunction can be represented as the union of the following three polyhedra

$$\mathcal{P}_{0,0,0}: \begin{cases} (\psi, z^+, z^-) = (0,0,0) \\ \delta\mathbf{p}^{\mathrm{f}} = 0 \\ \underline{\theta} \le \theta \le \bar{\theta} \end{cases} \tag{17}$$
$$\mathcal{P}_{1,1,0}: \begin{cases} (\psi, z^+, z^-) = (1,1,0) \\ \delta\underline{B} \cdot \theta \le \delta\mathbf{p}^{\mathrm{f}} \le \delta\bar{B} \cdot \theta \\ 0 \le \theta \le \bar{\theta} \end{cases} \tag{18}$$
$$\mathcal{P}_{1,0,1}: \begin{cases} (\psi, z^+, z^-) = (1,0,1) \\ \delta\bar{B} \cdot \theta \le \delta\mathbf{p}^{\mathrm{f}} \le \delta\underline{B} \cdot \theta \\ \underline{\theta} \le \theta \le 0 \end{cases} \tag{19}$$

where z^+, z^- are additional binary variables that capture the relationship between ψ, θ and $\delta\mathbf{p}^{\mathrm{f}}$. Namely, if $\psi = 0$, then z^+, z^- are both set to zero. Conversely, when $\psi = 1$, variable z^+ (resp. z^-) indicates whether the phase angle difference is positive (resp. negative), i.e., $\theta \ge 0$, (resp. ≤ 0).

The MILP formulation for the 3-term disjunction proposed in this paper (16) is given by

$$z^+ + z^- = \psi, \tag{20a}$$
$$\underline{\theta} z^+ + \theta \ge \underline{\theta}, \tag{20b}$$
$$\bar{\theta} z^- + \theta \le \bar{\theta}, \tag{20c}$$
$$-\bar{\theta}\,\delta\underline{B} z^+ - \underline{\theta}\,\delta\bar{B} z^- + \delta\mathbf{p}^{\mathrm{f}} \ge 0, \tag{20d}$$
$$-\bar{\theta}\,\delta\bar{B} z^+ - \underline{\theta}\,\delta\underline{B} z^- + \delta\mathbf{p}^{\mathrm{f}} \le 0, \tag{20e}$$
$$\bar{\theta}\,\delta\underline{B} z^+ + \bar{\theta}\,\delta\bar{B} z^- + \delta\bar{B}\theta - \delta\mathbf{p}^{\mathrm{f}} \le \bar{\theta}\,\delta\bar{B}, \tag{20f}$$
$$\bar{\theta}\,\delta\bar{B} z^+ + \bar{\theta}\,\delta\underline{B} z^- + \delta\underline{B}\theta - \delta\mathbf{p}^{\mathrm{f}} \ge \bar{\theta}\,\delta\underline{B}, \tag{20g}$$
$$\underline{\theta}\,\delta\bar{B} z^+ + \underline{\theta}\,\delta\underline{B} z^- + \delta\bar{B}\theta - \delta\mathbf{p}^{\mathrm{f}} \ge \underline{\theta}\,\delta\bar{B}, \tag{20h}$$
$$\underline{\theta}\,\delta\underline{B} z^+ + \underline{\theta}\,\delta\bar{B} z^- + \delta\underline{B}\theta - \delta\mathbf{p}^{\mathrm{f}} \le \underline{\theta}\,\delta\underline{B}, \tag{20i}$$
$$\psi, z^+, z^- \in \{0,1\}, \tag{20j}$$

and it is complemented by the big-M constraint

$$-(\bar{\mathbf{p}}^{\mathrm{f}} + m\Delta^c)\psi \le \delta\mathbf{p}^{\mathrm{f}} \le (\bar{\mathbf{p}}^{\mathrm{f}} + m\Delta^c)\psi, \tag{21}$$

which, although redundant with constraints (20), (9) and (4), was found to improve performance. The proposed strong TNEP+FACTS formulation is summarized in Model 3.

Model 3 The proposed TNEP+FACTS formulation

$$\min \quad \sum_{ij\in\mathcal{E}} c_{ij}^{\mathrm{cap}}\gamma_{ij} + c_{ij}^{\mathrm{TCSC}}\psi_{ij} + \frac{1}{S}\sum_{i\in\mathcal{N},s\in\mathcal{S}} c_i(\mathbf{p}_{i,s}^{\mathrm{g}}) + \lambda|\xi_{i,s}|$$

s.t. (1), (2) $\forall i \in \mathcal{N}, s \in \mathcal{S}$
(4), (5), (9) $\forall ij \in \mathcal{E}, s \in \mathcal{S}$
(20) $\forall ij \in \mathcal{E}, s \in \mathcal{S}$
(21) $\forall ij \in \mathcal{E}, s \in \mathcal{S}$

It is easy to verify, e.g., by explicit inspection of all three feasible realizations of ψ, z^+, z^-, that the feasible set of constraints (20) is exactly $\mathcal{P}_{0,0,0} \cup \mathcal{P}_{1,1,0} \cup \mathcal{P}_{1,0,1}$. This, in turn, proves the validity of the proposed formulation (Model 3). The strength of the formulation stems from the result of Theorem 1 below, which shows that every constraint in (20) is facet-defining, i.e., the constraints are as tight as possible.

Theorem 1. *The inequality constraints in* (20) *are facet-defining for* $\mathcal{P} = \mathrm{conv}(\mathcal{P}_{0,0,0} \cup \mathcal{P}_{1,1,0} \cup \mathcal{P}_{1,0,1})$.

Proof. First, observe that $\mathcal{P}$ is a 4-dimensional set because of the equality constraint $\psi = z^+ + z^-$. Therefore, every facet of $\mathcal{P}$ is a valid inequality for $\mathcal{P}$ which is tight at 4 extreme points. The rest of the proof follows by verifying that each inequality constraint in (20) is tight at least 4 extreme points of $\mathcal{P}$, using the extreme point characterization of Lemma 1. Note that $\psi \le 1$, $z^+ \ge 0$ and $z^- \ge 0$, which are a consequence of the binary requirement on ψ, z^+, z^-, are also facet-defining. □

Lemma 1. *The extreme points of $\mathcal{P}_{0,0,0}$, $\mathcal{P}_{1,1,0}$ and $\mathcal{P}_{1,0,1}$ are*

$$\mathcal{P}_{0,0,0} = \text{conv}\left\{ \begin{array}{l} (0,0,0,\underline{\theta},0), \\ (0,0,0,\bar{\theta},0) \end{array} \right\} \tag{22a}$$

$$\mathcal{P}_{1,1,0} = \text{conv}\left\{ \begin{array}{l} (1,1,0,0,0), \\ (1,1,0,\bar{\theta},\bar{\theta}\cdot\delta\underline{B}), \\ (1,1,0,\bar{\theta},\bar{\theta}\cdot\delta\bar{B}) \end{array} \right\} \tag{22b}$$

$$\mathcal{P}_{1,0,1} = \text{conv}\left\{ \begin{array}{l} (1,0,1,0,0), \\ (1,0,1,\underline{\theta},\underline{\theta}\cdot\delta\underline{B}), \\ (1,0,1,\underline{\theta},\underline{\theta}\cdot\delta\bar{B}) \end{array} \right\} \tag{22c}$$

Proof. Immediate by inspection. □

Finally, the paper implements a simple bound-tightening procedure to further strengthen the formulation. This strategy is applied as a pre-processing step, and it tightens lower and upper limits on each phase-angle difference. Namely, the approach uses the relation

$$\bar{\mathbf{p}}^{\text{f}} + m\Delta^c \geq \mathbf{p}^{\text{f}} = (B+\delta B)\theta \geq (B+\delta\underline{B})\theta \tag{23}$$

which yields $\theta \leq \min(\bar{\theta}, (\bar{\mathbf{p}}^{\text{f}} + m\Delta^c)(B+\delta\underline{B})^{-1})$ and allows the opportunity to tighten the upper limit on θ. The lower limit is tightened similarly.

III. Numerical results

A. Data generation

The paper reports numerical experiments on the 123-bus Texas 345kv backbone transmission system [13]. The system comprises 123 buses, 255 branches, 138 non-renewable generators, and 154 renewable (wind and solar) generators. The data provided in [13] also includes hourly time series of load and renewable generation. To reflect future systems with a high renewable penetration, the paper scales the load, wind and solar time series by 1.5, 2 and 3, respectively. This should give interesting case studies for how the Texas grid will evolve.

Figure 2 depicts the grid topology, which spans the state of Texas, and shows the location and size (scaled nameplate capacity, in MW) of each renewable generator. An important feature of the Texas system is that renewable generation is primarily located in the west of the state, where the wind resource is abundant, whereas load areas are concentrated around major metropolitan and industrial areas, especially Houston (south-east, by the coast) and Dallas (north-east).

The experiments consist of 10 scenarios for TNEP, each corresponding to one hour of the year. For both summer and winter, the experiments select the five hours corresponding to the highest load, highest net load, highest wind generation, highest solar generation, and lowest wind generation over that season. These hours are the most likely to lead to congestion, load shedding, and/or curtailment of renewable generation.

The production costs of non-renewable generators are taken from [13], and the cost of renewable generators is set to zero. Table I reports cost information regarding capacity upgrades, TCSC devices, and unserved/overserved energy penalties, which are adapted from [10]. There is little information available in the literature regarding the cost of TCSC devices. Preliminary experiments using the same cost data as reported in [10], resulted in no capacity upgrades nor FACTS device being installed, i.e., it was more economical to pay penalties for unserved energy. This suggests that the penalties in [10] might have been too low relative to the upgrade costs. Therefore, the authors elected to adjust penalties and investment costs to obtain more interesting test cases and more insights into potential upgrade scenarios.

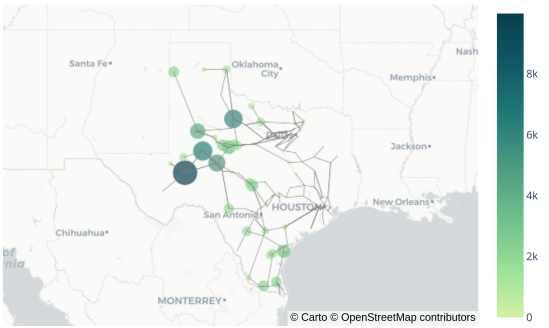

Fig. 2. The 123-bus Texas 345kV backbone topology. Circles indicate the location and size (scaled nameplate capacity, in MW) of renewable generators.

TABLE I
Cost Configuration

	Costs
Unserved & Overserved Energy	\$50,000/MWh
Capacity Upgrades	\$124/MW-km
TCSCs	\$2,200/MVA

B. Computational Performance

All TNEP formulations are implemented in Julia using the JuMP [14] modeling language. All experiments are executed on 24-core Intel Xeon machines running Linux, on the Phoenix cluster [15]. They are executed with 24 threads, 288GB of RAM, a 6-hour time limit, a 0.01% optimality gap tolerance, and other settings set to default.

Four TNEP formulations are compared:

1) TNEP: the baseline TNEP formulation of Model 1, which does not consider FACTS devices.
2) FBSM: the TNEP+FACTS formulation of Model 2 [12].
3) FBSMi: the improved FBSM formulation, with individual big-M values for individual branches.
4) FACeTS: the paper's formulation, presented in Model 3.

Experiments were conducted with two optimization solvers: Gurobi 10 [16], a commercial solver, and HiGHS [17], a leading open-source solver. Despite the comprehensive capabilities of HiGHS, it was unable to find good-quality solutions within the allocated 6-hour time limit, for any of the four formulations. Consequently, this study focuses on the results obtained through Gurobi, as it consistently provided results within the specified computational limits.

Table II reports, for each formulation: the number of variables (Vars), constraints (Constrs), and the corresponding compute time (Time, in seconds), and number of branch-and-bound nodes. The former two indicate the size of the

TABLE II
COMPARISON OF MILP FORMULATIONS

Formulation	Vars.	Constrs	Time	Nodes
TNEP	9,415	13,980	4s	156
FBSM [12]	14,770	29,280	1,733s	268,940
FBSMi	14,770	29,280	1,375s	253,954
FACeTS	17,320	36,930	386s	6,273

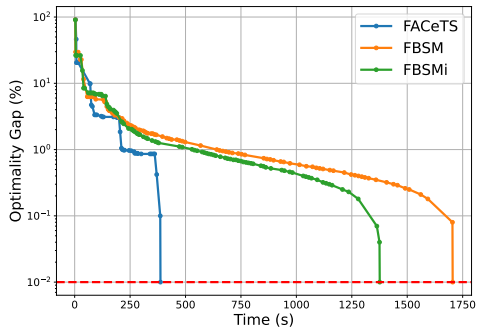

Fig. 3. Evolution of optimality gap (in %) over time, shown in log-scale. The **red** dashed line indicates the optimality tolerance of 0.01%.

problem, and the latter two metrics indicate the computational performance.

As expected, including FACTS devices significantly increases computing times, by a factor 100x–400x. The FBSM formulation performs the worst, with a computing time of 1,700s and over 260,000 branch-and-bound nodes needed to reach the prescribed optimality gap. The use of tighter big-M bounds yields a reduction in computing time of 20%, and marginal reduction in branch-and-bound nodes. *Despite comprising more variables and constraints, the FACeTS formulation yields the best performance, achieving a 4x speedup over FBSM, and an impressive 40x reduction in the number of branch-and-bound nodes.* This represents a key technical contribution of this paper.

Figures 3, 4 and 5 further depict the evolution of each formulation's optimality gap, primal bound and dual bound over time, respectively. The optimality gap after is defined as

$$gap = \frac{Z^p - Z^d}{|Z^p|},$$

where Z^p, Z^d denote the current primal and dual bounds. Figures 4 and 5 show that the computational speedup of FACeTS primarily arises from the enhancements of the dual bound. This improvement is a direct consequence of incorporating the facet-defining inequalities into the formulation, which serve to tighten the problem's relaxation through more precise cuts.

C. Transmission Expansion Results

Table III provides a detailed comparison of the physical performance between TNEP and TNEP+FACTS. The reported metrics include the final objective (Total Costs), line capacity upgrade costs, TCSC installation costs, nonrenewable

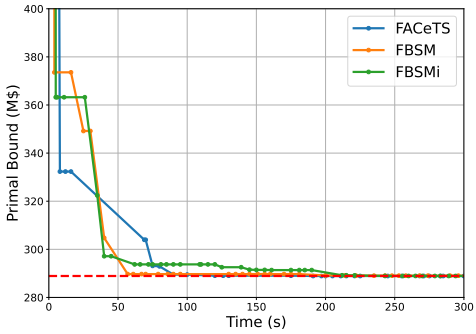

Fig. 4. Evolution of each formulation's primal bound (in M$) over time. The **red** dashed line indicates the optimal objective value.

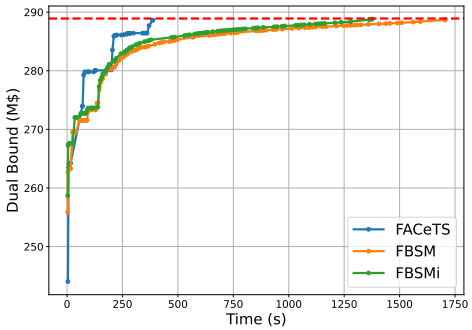

Fig. 5. Evolution of each formulation's dual bound (in M$) over time. The **red** dashed line indicates the optimal objective value.

TABLE III
COMPARISON OF PHYSICAL PERFORMANCE

Metric	TNEP	TNEP+FACTS
Total Costs (inc. penalties)	$296.20M	$288.91M
Capacity Upgrade Costs	$28.23M	$27.04M
TCSC Costs	-	$13.58M
Nonrenewable Costs	$1.86M	$1.84M
Unserved Energy	5322 MWh	4929 MWh
Curtailed Energy	8465 MWh	7408 MWh

generation costs, and the quantity of unserved energy and curtailed renewable energy. While the decline in total costs associated with the TNEP+FACTS approach is relatively modest, amounting to approximately 2.5%, there are notable advantages in other performance metrics. Specifically, the TNEP+FACTS methodology leads to a reduction of 393 MWh in unserved energy, i.e., a decrease of about 7.4%. Moreover, *curtailed renewable energy decreases by 1057 MWh, i.e., a reduction of nearly 12.5% compared to TNEP.*

Tables IV and V provide, for TNEP and TNEP+FACTS, respectively, a detailed breakdown of which branches are slated for capacity upgrades and, for TNEP+FACTS, where TCSCs devices are installed. Three levels of capacity upgrades (300MW, 600MW and 900MW) are available. While, at first glance, it might seem counterintuitive that TNEP+FACTS

TABLE IV
TNEP BRANCH INVESTMENTS

Type of Upgrade	Branch#	From Bus - To Bus
+300MW	151	San Antonio 14 - San Antonio 2
	166	San Antonio 2 - San Antonio 33
	183	Houston 12 - Houston 45
	188	Mexia - Frost
	194	Houston 48 - Pasadena 4
	250	Abilene 5 - Merkel 2
	251	Snyder 2 - Roscoe 2
+600MW	133	Blum - Frost
	247	Eastland - Gordon
+900MW	162	Mexia - Waco 2
	252	Throckmorton - Knox City
TCSCs	–	

TABLE V
TNEP+FACTS BRANCH INVESTMENTS

Type of Upgrade	Branch#	From Bus - To Bus
+300MW	101	Abilene 2 - Abilene 5
	151	San Antonio 14 - San Antonio 2
	166	San Antonio 2 - San Antonio 33
	183	Houston 12 - Houston 45
	188	Mexia - Frost
	194	Houston 48 - Pasadena 4
	251	Snyder 2 - Roscoe 2
	252	Throckmorton - Knox City
+600MW	133	Blum - Frost
	250	Eastland - Gordon
+900MW	162	Mexia - Waco 2
	247	Eastland - Gordon
TCSCs	72	Mccamey - Carlsbad
	197	Throckmorton - Knox City
	198	Throckmorton - Knox City
	235	North Richland Hills 1 - Weatherford 4
	248	Mccamey - Carlsbad

results in more line capacity upgrades, Table III reveals that the overall cost of line upgrades is lower compared to TNEP. Given that capacity upgrade costs are related to MW-km, this suggests that TNEP+FACTS capacity upgrades are predominantly occurring on shorter lines. The geographical distribution of these investments is shown in Figures 6 and 7, displaying TNEP and TNEP+FACTS investments, respectively. Red lines indicate the location of capacity upgrades, with the thickness/width of each line representing one of the three available upgrade levels. Figure 7 also shows TCSC installation locations, denoted by blue 'X's.

Figures 8 and 9 depict the location and amount of mean unserved energy for TNEP and TNEP+FACTS, respectively. A predominant portion of the unserved energy is observed near urban load centers. Notably, the integration of FACTS results in a pronounced reduction of unserved energy in the northern corridors. This aligns with the locations where the TCSCs were installed as seen in Figure 7.

Similarly, Figures 10 and 11 provide insight into the geographic distribution of mean curtailed energy. Notably, a significant portion of this curtailed energy is concentrated in

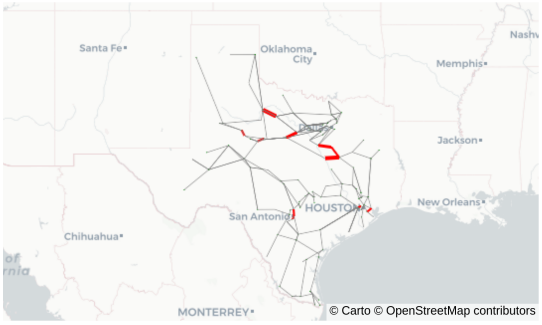

Fig. 6. Baseline TNEP Investments. **Red** lines indicate the location of capacity upgrades, with the thickness/width of each line representing one of the three available upgrade levels.

Fig. 7. TNEP+FACTS Investments. **Red** lines indicate the location of capacity upgrades, with the thickness/width of each line representing one of the three available upgrade levels. **Blue** 'X's indicate the location of installed TCSCs.

the western part of Texas, aligning with the areas of renewable capacity depicted in Figure 2. The inclusion of FACTS further leads to a tangible reduction in this curtailed energy.

In summary, by collectively analyzing the figures, it becomes evident that integrating FACTS to TNEP facilitates the transfer of renewable capacity to Texas's major urban centers.

IV. CONCLUSION

The paper has presented a novel MILP formulation for including FACTS devices in TNEP problems, which directly represents the change in power flow induced by FACTS devices. The proposed formulation enjoys strong theoretical guarantees, namely, it uses facet-defining constraints instead of weak big-M constraints as in previous formulations. Numerical experiments demonstrate the superiority of the proposed approach, which yields a 4x speedup and a 40x reduction in branch-and-bound nodes compared to state-of-the-art formulations. In addition, the results show that FACTS devices have the potential to reduce load shedding and renewable generation curtailment, by reducing congestion on the system.

Future work will explore the integration of energy storage technologies within the TNEP+FACTS framework, and conduct experiments across more detailed and larger-scale systems, for which further computational enhancements will likely be needed. Another interesting direction is to extend the proposed formulation to consider FACTS devices in unit commitment and economic dispatch problems, which underlie

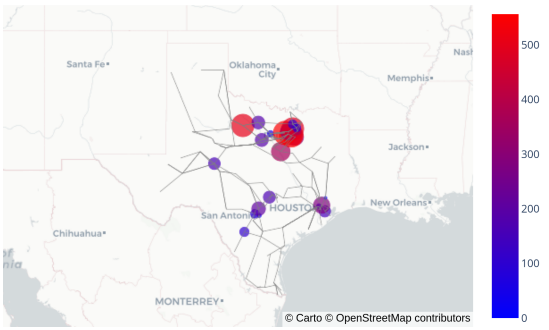

Fig. 8. Unserved energy in baseline TNEP. Circles indicate the location and amount (in MWh) of average unserved energy.

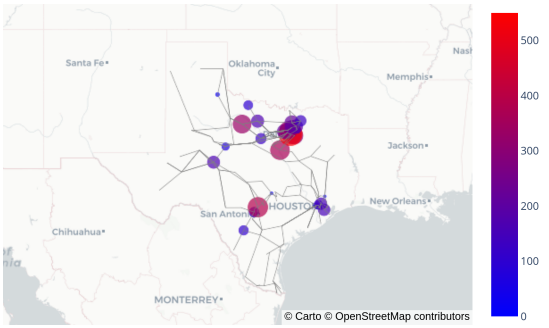

Fig. 9. Unserved energy in TNEP+FACTS. Circles indicate the location and amount (in MWh) of average unserved energy.

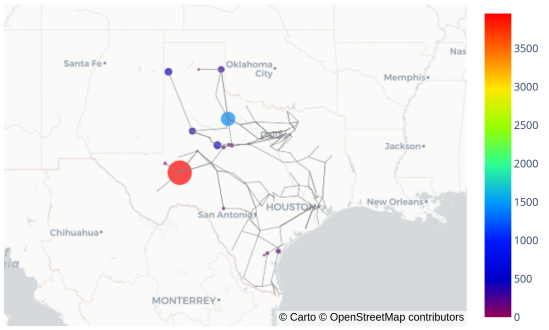

Fig. 10. Curtailed energy in baseline TNEP. Circles indicate the location and amount (in MWh) of average curtailed energy.

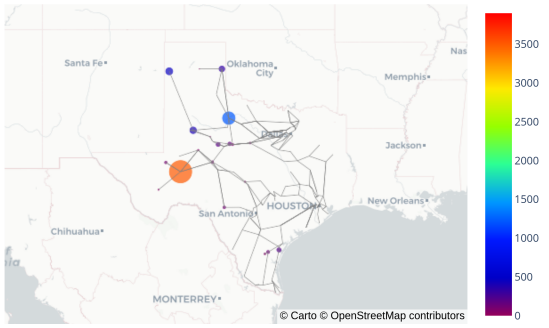

Fig. 11. Curtailed energy in baseline TNEP. Circles indicate the location and amount (in MWh) of average curtailed energy.

most day-ahead and real-time electricity markets in the US. Tractable formulations for such problems would allow for more efficient markets, and expand the set of control actions available to operators in real-time, showcasing the potential for improved reliability and efficiency of power systems.

References

[1] Réseau de Transport d'Électricité, "Energy Pathways to 2050," Réseau de Transport d'Électricité, Tech. Rep., 2022.

[2] N. Gideon Ude, H. Yskandar, and R. Coneth Graham, "A comprehensive state-of-the-art survey on the transmission network expansion planning optimization algorithms," *IEEE Access*, vol. 7, pp. 123 158–123 181, 2019.

[3] M. S. Mokhtari, M. Gitizadeh, and M. Lehtonen, "Optimal coordination of thyristor controlled series compensation and transmission expansion planning: Distributionally robust optimization approach," *Electric Power Systems Research*, vol. 196, p. 107189, 2021.

[4] C. Li, A. J. Conejo, P. Liu, B. P. Omell, J. D. Siirola, and I. E. Grossmann, "Mixed-integer linear programming models and algorithms for generation and transmission expansion planning of power systems," *European Journal of Operational Research*, vol. 297, no. 3, pp. 1071–1082, 2022.

[5] G. Micheli, M. T. Vespucci, M. Stabile, C. Puglisi, and A. Ramos, "A two-stage stochastic milp model for generation and transmission expansion planning with high shares of renewables," *Energy Systems*, pp. 1–43, 2020.

[6] S. Lumbreras and A. Ramos, "Transmission expansion planning using an efficient version of benders' decomposition. a case study," in *2013 IEEE Grenoble Conference*. IEEE, 2013, pp. 1–7.

[7] X. Blanchot, F. Clautiaux, A. Froger, and M. Ruiz, "Solving a bilevel stochastic generation and transmission expansion planning problem," 2023, preprint available on HAL-Inria: https://hal-lirmm.ccsd.cnrs.fr/INRIA/hal-03957750v1.

[8] R. A. de Araujo, S. P. Torres, J. Pissolato Filho, C. A. Castro, and D. Van Hertem, "Unified ac transmission expansion planning formulation incorporating vsc-mtdc, facts devices, and reactive power compensation," *Electric Power Systems Research*, vol. 216, p. 109017, 2023.

[9] Z. Luburić, H. Pandžić, and M. Carrión, "Transmission expansion planning model considering battery energy storage, TCSC and lines using AC OPF," *IEEE Access*, vol. 8, pp. 203 429–203 439, 2020.

[10] M. Esmaili, M. Ghamsari-Yazdel, N. Amjady, C. Chung, and A. J. Conejo, "Transmission expansion planning including tcscs and sfcls: A minlp approach," *IEEE Transactions on Power Systems*, vol. 35, no. 6, pp. 4396–4407, 2020.

[11] O. Ziaee, O. Alizadeh-Mousavi, and F. F. Choobineh, "Co-optimization of transmission expansion planning and tcsc placement considering the correlation between wind and demand scenarios," *IEEE Transactions on Power Systems*, vol. 33, no. 1, pp. 206–215, 2017.

[12] M. Franken, H. Barrios, A. B. Schrief, and A. Moser, "Transmission expansion planning via power flow controlling technologies," *IET Generation, Transmission & Distribution*, vol. 14, no. 17, pp. 3530–3538, 2020.

[13] J. Lu, "Tx-123bt network model," 2023. [Online]. Available: https://rpglab.github.io/resources/TX-123BT/

[14] M. Lubin, O. Dowson, J. Dias Garcia, J. Huchette, B. Legat, and J. P. Vielma, "JuMP 1.0: Recent improvements to a modeling language for mathematical optimization," *Mathematical Programming Computation*, 2023.

[15] PACE, *Partnership for an Advanced Computing Environment (PACE)*, 2017. [Online]. Available: http://www.pace.gatech.edu

[16] Gurobi Optimization, LLC, "Gurobi Optimizer Reference Manual," 2023. [Online]. Available: https://www.gurobi.com

[17] Q. Huangfu and J. J. Hall, "Parallelizing the dual revised simplex method," *Mathematical Programming Computation*, vol. 10, no. 1, pp. 119–142, 2018.